Petroleum Science 22 (2025) 2493–2501

Contents lists available at ScienceDirect

Petroleum Science

journal homepage: www.keaipublishing.com/en/journals/petroleum-science

Original Paper

Dynamic characterization of viscoelasticity during polymer flooding: A two-phase numerical well test model and field study

Yang Wang [a, *], Shi-Long Yang [a], Hang Xie [a], Yu Jiang [b], Shi-Qing Cheng [a], Jia Zhang [a, **]

[a] State Key Laboratory of Petroleum Resources and Engineering, China University of Petroleum (Beijing), Beijing, 102249, China
[b] Itasca Consulting Group, Inc., Minneapolis, 55401, United States

ARTICLE INFO

Article history:
Received 22 July 2024
Received in revised form
27 April 2025
Accepted 28 April 2025
Available online 29 April 2025

Edited by Yan-Hua Sun

Keywords:
Polymer flooding
Two-phase flow
Numerical well test model
Viscoelastic characteristic
Nonlinear flow
Near-well blockage

ABSTRACT

Polymer flooding is an important means of improving oil recovery and is widely used in Daqing, Xinjiang, and Shengli oilfields, China. Different from conventional injection media such as water and gas, viscoelastic polymer solutions exhibit non-Newtonian and nonlinear flow behavior including shear thinning and shear thickening, polymer convection, diffusion, adsorption, retention, inaccessible pore volume, and reduced effective permeability. However, available well test model of polymer flooding wells generally simplifies these characteristics on pressure transient response, which may lead to inaccurate results. This work proposes a novel two-phase numerical well test model to better describe the polymer viscoelasticity and nonlinear flow behavior. Different influence factors that related to near-well blockage during polymer flooding process, including the degree of blockage (inner zone permeability), the extent of blockage (composite radius), and polymer flooding front radius are explored to investigate these impacts on bottom hole pressure responses. Results show that polymer viscoelasticity has a significant impact on the transitional flow segment of type curves, and the effects of near-well formation blockage and polymer concentration distribution on well test curves are very similar. Thus, to accurately interpret the degree of near-well blockage in injection wells, it is essential to first eliminate the influence of polymer viscoelasticity. Finally, a field case is comprehensively analyzed and discussed to illustrate the applicability of the proposed model.

1. Introduction

As a mature and economically viable tertiary oil recovery technology, polymer flooding has been widely applied in major oil fields in China, such as Daqing, Xinjiang, and Shengli oilfields, achieving significant results in increasing oil production and reducing water content (Seright and Wang, 2023; Wang et al., 2024). Unlike conventional injection media (such as water and gas), viscoelastic polymer solutions exhibit shear thinning and shear thickening properties when flowing through porous media. The viscosity of these solutions varies significantly under different shear rates, resulting in highly nonlinear flow equations (Azad and Trivedi, 2019; Shende et al., 2021). Additionally, due to the adsorption and retention of polymer molecules and solid particles carried during polymer flooding, pore volume may decrease and effective permeability may decline, further complicating the flow characteristics of polymer flooding. Well testing, an important method for reservoir engineering analysis and exploitation study, is one of the most straightforward and economical techniques for obtaining reservoir parameters and is widely used in polymer flooding (Gringarten, 2008; Wang et al., 2019).

From 1964 to 1971, Pye (1964), Marshall and Metzner (1967), Smith (1970), and Jennings et al. (1971) discovered that high molecular weight polymers can significantly reduce water phase mobility in porous media. To address this phenomenon, Bondor et al. (1972) and Hirasaki and Pope (1974) proposed apparent viscosity models for high molecular weight polymers under different shear rates, including Newtonian fluid models, pseudoplastic fluid models, and viscoelastic fluid models. Masuda et al. (1992) established a new polymer viscoelastic viscosity model and verified its accuracy through core experiments. Yang et al. (2010) used a power-law model to describe the viscosity of viscoelastic polymers and, based on this, established a polymer flooding well testing model under single-phase flow conditions. They solved the flow equations using the finite difference method and performed

* Corresponding author.
** Corresponding author.
E-mail addresses: petroyang@163.com (Y. Wang), 651718766@qq.com (J. Zhang).

https://doi.org/10.1016/j.petsci.2025.04.029

sensitivity analysis on typical well testing curves. However, in calculating shear rates, they assumed an approximately linear relationship between flow velocity and flow rate, and neglected the effects of polymer convection, diffusion, adsorption, retention, and inaccessible pore volume. Yang (2011) established a viscoelastic polymer flooding well testing model and obtained numerical solutions using the finite difference method. However, this model also assumed an approximately linear relationship between flow velocity and flow rate and neglected the effects of polymer diffusion, adsorption, retention, and inaccessible pore volume. Liang et al. (2016) used viscoelastic constitutive equations to characterize the effective viscosity of polymer solutions. Under single-phase flow conditions, he established a viscoelastic polymer flooding well testing model and obtained numerical solutions using the finite difference method, exploring the impact of polymer elasticity on the shape of well testing curves in low-permeability reservoirs. However, he did not analyze the impact of polymer shear thickening on well testing in medium to high permeability reservoirs. This model also simplified the calculation of shear rates and neglected the effects of convection, diffusion, adsorption, retention, and inaccessible pore volume. Ma and McClure (2017) established a polymer flooding flow model considering polymer concentration distribution, shear thickening, and shear thinning under single-phase flow conditions, and obtained numerical solutions. They found that shear thickening behavior affects the early shut-in pressure of injection wells, but did not further explore the impact of polymer shear thickening characteristics on well testing interpretation. Xie et al. (2020) established a polymer flooding well testing model under single-phase flow conditions, considering the effects of polymer convection, diffusion, and adsorption based on the viscoelastic polymer viscosity model proposed by Masuda et al. (1992), and obtained approximate analytical solutions. However, this model neglected the impact of shear viscosity and simplified the calculation of shear rates.

In polymer flooding reservoirs in China, it has been found that a significant number of polymer injection wells face difficulties in injection and abnormal increases in injection pressure. This prevents them from meeting the requirements for regular or intermittent injection, severely affecting the efficiency of polymer flooding. The cause of this issue is blockages in the wellbore or the formation near the wellbore. Dauben and Menzie (1967) discovered during their study of polymer flooding that prolonged polymer injection leads to a significant increase in injection pressure. However, they did not investigate this phenomenon further at the time, attributing it to the residual resistance factor related to permeability. Lake et al. (2014) studied the migration of incompletely dissolved polymers in the formation, noting that the undissolved portions tend to deposit and remain in the reservoir, thus reducing the flow ability of the polymer solution. Li et al. (2016) suggested that the injected or produced fluid might scour rock particles or carry impurities into the formation. Based on this, he hypothesized that the skin factor changes over time and developed a mathematical model for well test interpretation, obtaining an analytical solution and conducting field test interpretations for verification. Qu et al. (2019) established a quantitative predictive analytical model for the polymer flooding blockage radius using well testing technology and reservoir engineering methods. Kamal et al. (2019) developed an analytical solution of bottom-hole pressure by combining the non-Newtonian fluids and the multi-composite reservoir models. The solution addresses the polymer region, where the fluids follow either the power law or Meter's model (Meter and Bird, 1964), and the Newtonian flow in the oil or water regions ahead of the polymer, with varying Newtonian- and non-Newtonian-fluid saturations in both regions.

The research findings indicate that existing studies primarily focus on analytical well testing methods for polymer flooding. However, these methods are insufficient to meet the demands of on-site well test analysis in oilfields. This is because the following. (1) Analytical well testing relies on solving flow equations to provide analytical solutions under ideal conditions and specific boundary conditions. It cannot handle complex reservoirs with irregular boundaries and heterogeneity, and accurately solve multiphase flow problems. (2) Current models simplify polymers as power-law fluids, and have not comprehensively considered the impact of complex polymer behavior in polymer flooding well testing (Yang et al., 2010; Liang et al., 2016; Ma and McClure, 2017; Xie et al., 2020).

In this paper, an oil–water two-phase flow numerical well testing model is established considering the comprehensive effects of shear thickening, shear thinning, convection, diffusion, adsorption, retention, inaccessible pore volume, and reduced reservoir permeability caused by polymer solution in the porous media. The degree and extent of formation blockage, and polymer flooding front radius on the bottom-hole pressure responses are detailed explored. Finally, a field case is discussed to explore the complicated polymer characteristics on pressure behavior, and further validate the applicability of proposed model.

2. Methodology

2.1. Physical model

The basic assumptions of the viscoelastic polymer flooding reservoir model are as follows:

(1) The reservoir is isotropic, isothermal, and of uniform thickness, with uniform initial reservoir pressure, water saturation, and polymer concentration distribution.
(2) The reservoir fluid contains oil and water, with polymers dissolved in the water phase. No chemical reactions occur during polymer flooding.
(3) The flow of oil and water phases in the reservoir obeys Darcy's law.
(4) Shear thickening, shear thinning, convection, diffusion, adsorption, and retention of polymers are considered. The model takes into account the permeability reduction of water phase caused by polymers and the inaccessible pore volume due to the large molecular structure of polymers.
(5) The influences of oil and water relative permeability and capillary pressure are considered.
(6) Both the rock and fluid in the reservoir have slight compressibility.

2.2. Mathematical model

The partial differential equations for oil, water, and polymer flow are established based on the assumptions mentioned above

$$\frac{\partial}{\partial t}(\phi b_\alpha S_\alpha) + \nabla\cdot(b_\alpha \boldsymbol{v}_{\boldsymbol{\alpha}}) - Q_\alpha = 0, \quad \alpha = \{\mathrm{o},\ \mathrm{w}\} \tag{1}$$

$$\frac{\partial}{\partial t}\left[\phi f_\mathrm{p} b_\mathrm{w}\left(S_\mathrm{w} C_\mathrm{p} + \hat{C}_\mathrm{p}\right)\right] + \nabla\cdot(b_\mathrm{w}\boldsymbol{v}_{\mathbf{w}} C_\mathrm{p}) + \nabla\cdot(\boldsymbol{v}_\mathrm{d}) - Q_\mathrm{w} C_\mathrm{p} = 0 \tag{2}$$

where α refers to oil or gas phase, subscripts o and w represent oil and water, respectively; t is the time; $\boldsymbol{v}_\alpha$ is the flow rate of oil or water; Q_α is the oil or water rate in the wellbore; ϕ is porosity; b_α is

the reciprocal of oil or water volume factor; S_α is the oil or water saturation; C_p is the injected polymer concentration; $\hat{C}_p$ is the adsorption concentration of polymer in the reservoir; $\boldsymbol{v}_d$ is the polymer diffusion rate in the water phase.

In the polymer flooding process, the large molecular structure of polymers prevents them from entering some reservoir pores. Therefore, the coefficient representing the accessible pore volume of the polymer, denoted as f_p, is added in Eq. (2). This coefficient represents the ratio of the accessible pore volume of the polymer to the total pore volume of the reservoir rock. The polymer adsorption concentration can be characterized by the Langmuir adsorption equation as

$$\hat{C}_p = \frac{\hat{C}_{pmax} b_p C_p}{1 + b_p C_p} \tag{3}$$

where $\hat{C}_{pmax}$ is the maximum adsorption concentration of polymer; b_p is a constant.

The flow of the oil and water in the porous media obeys Darcy's law. Meanwhile, the relative permeability and permeability reduction of water phase are also considered. Therefore, the flow rates of the oil and the water phases can be written as

$$\boldsymbol{v}_o = -\frac{\boldsymbol{K} k_{ro}}{\mu_o}(\nabla p_o) \tag{4}$$

$$\boldsymbol{v}_w = -\frac{\boldsymbol{K} k_{rw}}{\mu_{weff} R_k}(\nabla p_w) \tag{5}$$

The polymer diffusion rate in the water phase can be characterized as

$$\boldsymbol{v}_d = -\boldsymbol{D}_p \phi f_p S_w (\nabla C_p) \tag{6}$$

where $\boldsymbol{K}$ is the absolute permeability; $k_{r\alpha}$ is the relative permeability of oil or water phase; p_α is the pressure of oil or water phase; μ_o is the oil viscosity; μ_{weff} is the effective viscosity of water phase; R_k is the effective water permeability decline coefficient; $\boldsymbol{D}_p$ is the polymer diffusion coefficient.

The permeability reduction of water phase can be characterized by the formula proposed by Hou et al. (2003) as

$$R_k = 1 + \frac{(R_{kmax} - 1) b_p C_p}{1 + b_p C_p} \tag{7}$$

where R_{kmax} is the maximum permeability reduction coefficient.

To calculate the apparent viscosity of the water phase in viscoelastic polymer flooding process, the unified viscosity model for polymer solutions proposed by Delshad et al. (2008) is adopted in this study. This model is capable of characterizing both the shear viscosity and extensional viscosity of polymers as follows

$$\mu_{weff} = \mu_{sh} + \mu_{el} \tag{8}$$

with

$$\mu_{sh} = \mu_w + \left(\mu_p^0 - \mu_w\right)\left[1 + (\lambda_1 \gamma)^2\right]^{\frac{n_1 - 1}{2}}$$

$$\mu_{el} = \mu_{max}\left\{1 - \exp\left[-(\lambda_2 \tau_r \gamma)^{n_2 - 1}\right]\right\}$$

where μ_{sh} is the shear viscosity of polymer; μ_{el} is the elongational viscosity of polymer; μ_w is the water viscosity; γ is the shear rate of polymer; μ_p^0 is the zero shear viscosity of polymer; τ_r is the relaxation time of polymer; μ_{max} is the empirical constant; n_1, n_2, λ_1, λ_2 are also empirical constants for calculating polymer viscosity.

During the well testing, the total flow rate is known, which is the sum of the flow rates of the oil phase and the water phase in the wellbore.

$$Q_s = \sum (Q_w + Q_o) \tag{9}$$

According to Darcy's law, the flow rates of oil and water phase are

$$Q_\alpha = \frac{2\pi |\boldsymbol{K}| \lambda_\alpha h b_\alpha}{(\ln(r_e/r_w) + S)}\left(p_{wf} - p_\alpha\right) + C b_\alpha \frac{dp_{wf}}{dt} \tag{10}$$

with

$$\lambda_o = \frac{k_{ro}}{\mu_o}$$

$$\lambda_w = \frac{k_{rw}}{\mu_{weff} R_k}$$

where Q_s is the flow rate in the wellbore; h is the formation thickness; r_e is the outer boundary radius; r_w is the wellbore radius; S is the skin factor; p_{wf} is the bottom hole pressure; C is the wellbore-storage coefficient.

To solve the equations, initial and boundary conditions are also required. The initial conditions are

$$p_o(x, y, z, 0) = p_i \tag{11}$$

$$S_w(x, y, z, 0) = S_{wi} \tag{12}$$

$$C_p(x, y, z, 0) = C_{pi}(x, y, z) \tag{13}$$

The boundary conditions are

$$\left.\frac{\partial p_o}{\partial x}\right|_{x=0, x_{max}} = \left.\frac{\partial p_o}{\partial y}\right|_{y=0, y_{max}} = \left.\frac{\partial p_o}{\partial z}\right|_{z=0, z_{max}} = 0 \tag{14}$$

The auxiliary equations include the saturation equation and the capillary pressure equation, which are

$$S_w + S_o = 1 \tag{15}$$

$$p_{cow} = p_w - p_o \tag{16}$$

where x, y, z are the coordinates; x_{max}, y_{max}, z_{max} are the maximum coordinate values in the x, y, z directions; p_i is the initial reservoir pressure; S_{wi} is the initial water saturation; C_{pi} is the initial polymer concentration; p_{cow} is the capillary pressure.

The accurate computation of the effective viscosity of polymer is pivotal for ensuring the precision of the entire equation set. It is worth noting that the effective viscosity of the water phase (referred to as the effective viscosity of the polymer solution) is a function of both polymer concentration and shear rate, which undergoes significant changes during the polymer flooding process. Wang et al. (2024) showed that the viscosity of polymer solution decreases continuously first, and then shows an upward trend as the increase in shear rate. In addition, it is required to maintain a stable injection rate as much as possible before shutting in the well in the practice of well testing. Therefore, Newton's iteration method is employed to initialize and iteratively calculate the shear rate in each iteration step, ensuring the stability and accuracy of its calculation.

2.3. Model validation

To validate the reliability of the numerical solution of the viscoelastic polymer flooding well test model, we compare our model with commercial numerical simulation software. Fig. 1 illustrates the grid of the polymer flooding reservoir model, with dimensions of 300 m × 300 m × 10 m, containing one polymer injection well and one production well, spaced at 141.42 m apart. The vicinity of the wells is represented by radially refined PEBI grids, with a minimum grid radius of 1.24 m; while the distant well zones are characterized by Cartesian grids, with a single grid size of 10 m × 10 m × 10 m. In the commercial numerical simulation software (CMG) used for comparison, a Cartesian grid of 300 m × 300 m × 10 m is established, with a single grid size of 2 m × 2 m × 2 m, and the well positions are arranged the same as in Fig. 1. Assume the permeability of this case is 100×10^{-3} μm^2, and the porosity is 30%. Initial reservoir pressure is 20 MPa. Rock compressibility is 0.001 MPa^{-1}. Initial water saturation is 65%. Oil viscosity is 7.41 mPa·s. Oil compressibility is 0.001 MPa^{-1}. Water compressibility is 0.0002 MPa^{-1}. Constant parameter (b_p) is 2.27. Maximum permeability reduction factor (R_{kmax}) is 1.84. The relative permeability curves are shown in Fig. 2, and the capillary force curve is shown in Fig. 3. It is assumed that the injection rate of the injector and the production rate of the producer are both 100 m^3/d, the injected polymer concentration is 0.5 kg/m^3, and the simulation time is 300 d. As shown in Fig. 4, the comparison results show that the bottom hole pressures computed from the two approaches have a good agreement, which indicates the accuracy of our model.

3. Pressure transient analysis of polymer flooding wells for near-well blockage

In polymer flooding reservoirs, near-well blockages often occur in injection wells (see Fig. 5), resulting in abnormally high injection pressure and injection difficulties. Near-well blockages in injection wells can generally be divided into two parts based on the location of blockage: the increase in skin factor caused by filter cake around the wellbore, and the decrease in reservoir permeability in the near-well zone due to the migration, adsorption, and retention of polymers, minerals, and impurities. Due to its efficiency and cost-effectiveness, pressure falloff test in polymer injection wells is one of the common methods to assess the degree and extent of blockage. Although the heterogeneity of the reservoir can be considered in our model, it is generally assumed homogeneous and isotropic in the practical applications. Otherwise, too many unknowns will lead to strong ambiguity in parameter interpretation. Please note that well testing does not care about changes in reservoir parameters and blockage radius. It only determines the parameters at that moment by shutting the well and measuring the pressure data.

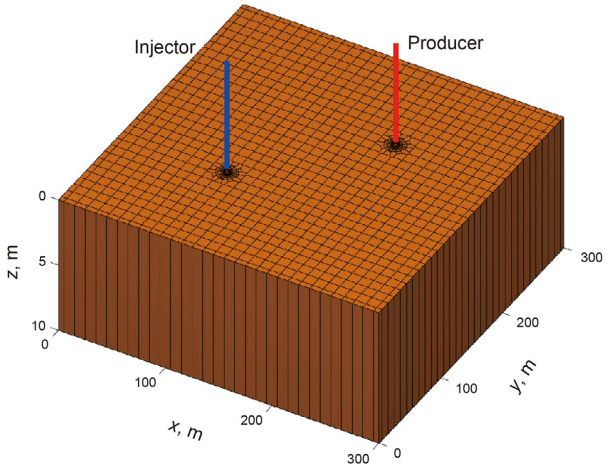

Fig. 1. Grid system of a reservoir with polymer flooding.

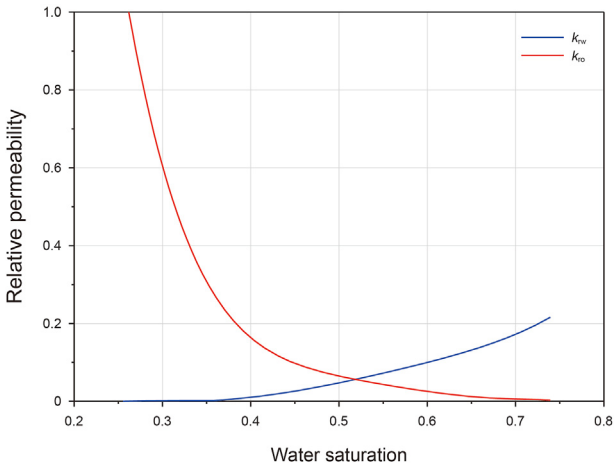

Fig. 2. The relative permeability curves.

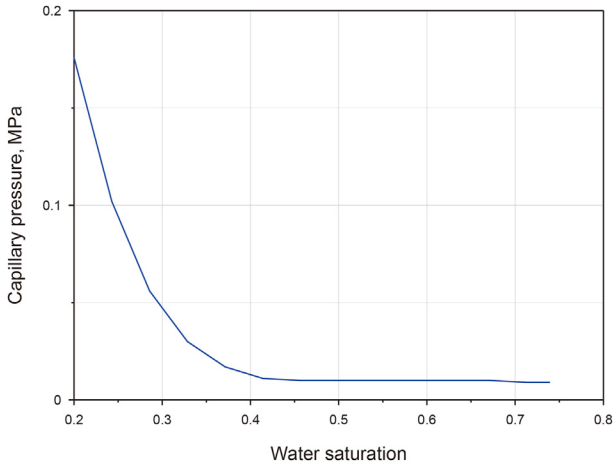

Fig. 3. The capillary pressure curve.

In this model, the inputs include wellbore radius, pay zone, rock compressibility, water compressibility, water saturation, porosity, formation/oil/water volume factor, oil/water viscosity, relative permeability, the parameters to calculate polymer viscosity, polymer injection concentration, injection rate and measured bottom-hole pressure, and the outputs include wellbore-storage coefficient, skin factor, permeability (inner and outer permeability), blockage radius, polymer flooding front radius, reservoir pressure, and so on. Based on the mathematical equations (from Eqs. (1)–(16)) listed above, the theoretical bottom-hole pressure is calculated by assigning the initial values to the output parameters presented above. Then, the measured data is matched with the theoretical pressure data by adjusting the output parameters on the log-log curve. This analysis will complete until both the log-log curve and the historical pressure curve are matched.

In this section, the sensitivity analysis of the parameters related to near-well blockages (see Fig. 6) are conducted based on the viscoelastic polymer flooding well test model, which includes the

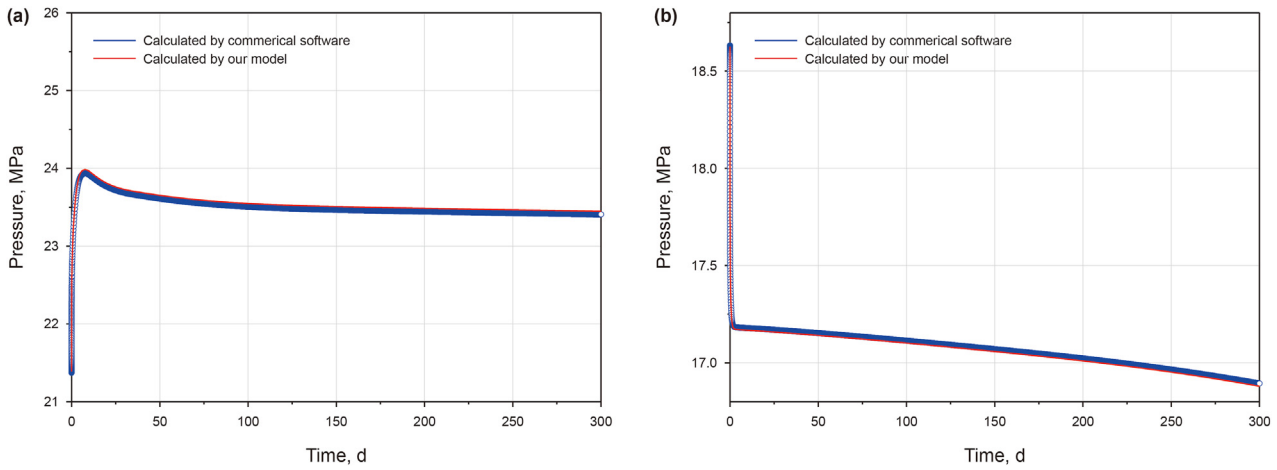

Fig. 4. Comparison between the numerical solution of the model in this paper and the commercial reservoir simulator. (**a**) Polymer injection well; (**b**) production well.

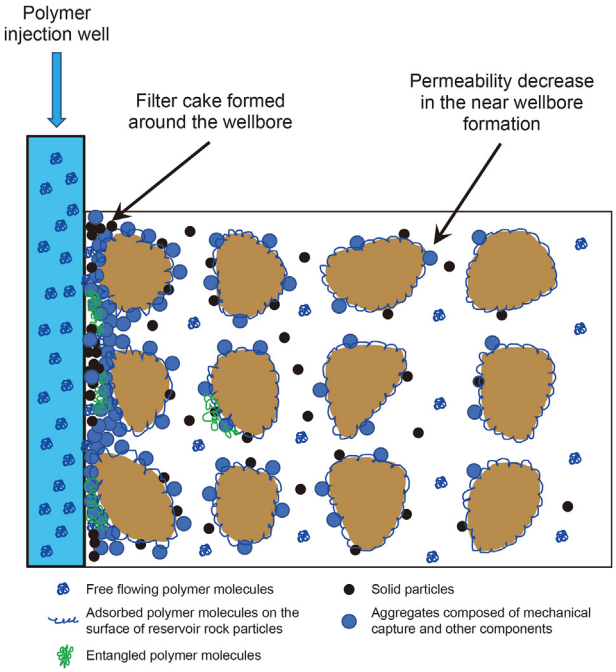

Fig. 5. Schematic of plugging in the region near the polymer injection well.

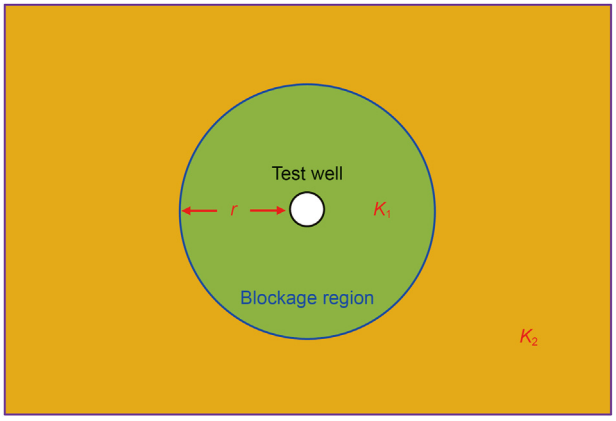

Fig. 6. Schematic of plugging in the formation near a polymer injection well.

degree of blockage (inner zone permeability) and the extent of blockage (composite radius). Additionally, considering the formation of polymer concentration gradients during continuous injection, sensitivity analysis is also performed on polymer flooding front radius.

Suppose a reservoir system with dimensions of 6000 m × 6000 m × 10 m is analyzed to assess the influence of near-well formation blockage and polymer concentration on the pressure transient response in the pressure falloff test. Different pressure curves for injection wells are plotted based on various blockage radii, inner zone permeabilities (i.e., degree of blockage), and polymer flooding front radii. The injection rate of the injection well is 100 m^3/d. The basic reservoir input parameters are same with the data in Section 2.3. The relative permeability curves and capillary pressure curves are illustrated in Figs. 2 and 3, respectively.

In cases with different blockage radii and degrees of blockage (K_1), the outer zone permeability (K_2) is 100 × 10^{-3} μm^2, and the injection concentration is 0.5 kg/m^3. The influence of blockage radius on bottom hole pressure behavior is shown in Fig. 7. Taking the $r = 33.83$ case as an example, the flow includes wellbore storage regime, transitional flow regime, radial flow regime of inner zone (polymer flooding radial flow segment), transitional flow regime, and radial flow regime of outer zone. It can be found that the characteristics of the polymer flooding radial flow segment

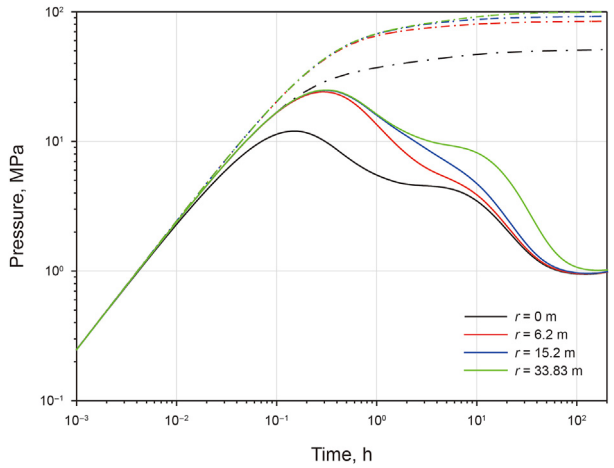

Fig. 7. Pressure falloff test curves of polymer injection wells with different blockage radii.

disappear as the blockage radius (r) increases. When the blockage radius reaches 33.83 m, the blocked area has reached near the polymer flooding front (this 33.83 m is obtained by the simulation of our model), and the characteristics of the polymer flooding radial flow segment reappear. As the inner zone permeability decreases, the characteristics of the polymer flooding radial flow gradually disappear. This is because when the inner zone permeability decreases to a certain extent, its impact on conductivity becomes greater than that of polymer concentration, masking the pressure response characteristics caused by differences in polymer concentration (see Fig. 8).

In the case with different polymer flooding fronts, the inner zone permeability (K_1) is 50 × 10^{-3} μm^2, the outer zone permeability (K_2) is 100 × 10^{-3} μm^2, the blockage radius is 33.83 m, and the injection concentration is 0.5 kg/m^3. It shows that the transitional range of the near-well formation blockage decreases, and the range of the radial flow segment corresponding to the polymer control zone gradually increases with the increase in the polymer flooding front radius (Fig. 9).

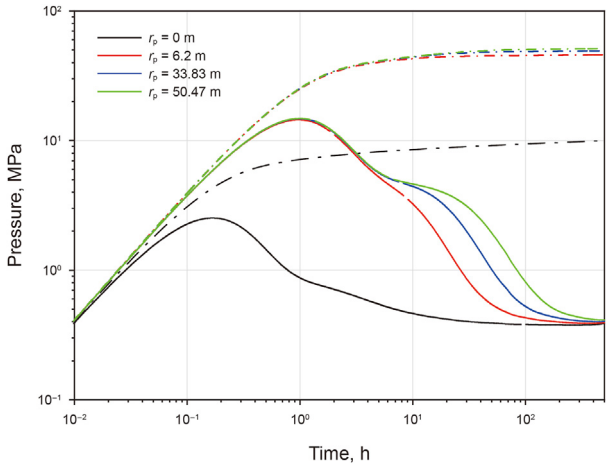

Fig. 9. Pressure falloff test curves of polymer injection wells with different polymer flooding fronts.

4. Field study

The sensitivity analysis in viscoelastic polymer flooding well testing has shown that polymer viscoelasticity has a significant impact on the transitional flow segment of type curves. When analyzing the impact of wellbore filter cake on pressure responses, the influence of polymer viscoelasticity should be considered. The sensitivity analysis of type curves for near-well formation blockage in injection wells has indicated that the effects of near-well formation blockage and polymer concentration distribution on well test curves are similar. Consequently, to accurately interpret the degree of near-well blockage in injection wells, it is essential to first consider the influence of polymer viscoelasticity. Subsequently, based on the concentration distribution, the degree and extent of formation blockage in the near-well zone can be interpreted. The specific process involves:

(1) Initially, conducting a preliminary history matching using the viscoelastic polymer flooding well test model to obtain the initial reservoir permeability.
(2) Then, based on the initial permeability, average injection concentration, and injection rate before shutting in the well, simulating the injection process to determine the approximate range of concentration distribution, thus reducing the ambiguity in well test interpretation.
(3) Finally, refining the interpretation of well test data using the viscoelastic polymer flooding well test model by adjusting the degree and radius of blockage and fine-tuning the polymer flooding front radius to obtain the final interpretation results.

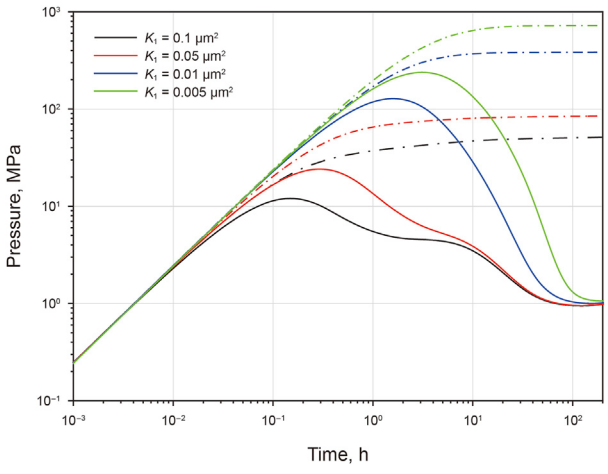

Fig. 8. Pressure falloff test curves of polymer injection wells with different inner zone permeabilities.

To illustrate the applicability of our model, an example from the literature of Zhang et al. (2021) is discussed. In Zhang et al.'s paper, he introduced this case to highlight the shear thickening behavior on bottom hole pressure responses. Here we will work step further on this example to explore the necessity of considering polymer viscoelasticity in well test interpretation and the superiority of our viscoelastic polymer flooding numerical well test model in identifying near-well blockage in injection wells.

The basic parameters of a polymer flooding well pressure falloff test are presented in Table 1. Near the injection well, there are no faults or bottom water, and there is observed anomalous pressure buildup before well testing. The relative permeability curves and capillary pressure curves are illustrated in Figs. 2 and 3, respectively. The date of the injection well shut-in pressure falloff test is October 14, 2015, with a cumulative injection time before shut-in of 302.7 d and an effective shut-in time of 71.46 h.

Four different well test models were applied and compared for well test interpretation as follows:

Model A: This model neglects shear-thickening properties and

Table 1
Basic parameters of a field case for polymer flooding falloff test (Zhang et al., 2021).

Parameter	Value
Porosity, %	17.4
Average permeability, 10^{-3} μm^2	786
Rock compressibility, MPa^{-1}	1.46 × 10^{-3}
Formation thickness, m	13
Well radius, m	0.07
Initial water saturation, %	64.9
Water viscosity, mPa·s	0.99
Oil viscosity, mPa·s	7.41
Water compressibility, MPa^{-1}	1.5 × 10^{-4}
Oil compressibility, MPa^{-1}	2 × 10^{-3}
Water volume factor, m^3/m^3	1.001
Oil volume factor, m^3/m^3	1.174
Injection rate of tested well, m^3/d	60
Polymer injection concentration, kg/m^3	0.503

assumes different polymer flooding front radii and blockage radii.

To illustrate the importance of polymer concentration distribution in identifying near-well formation blockage in injection wells, the following models were designed while considering shear-thinning and shear-thickening characteristics of the polymer.

Model B: Polymer concentration is uniformly distributed.

Model C: Polymer flooding front radius is the same as the blockage radius.

Model D: Polymer flooding front radius is different from the blockage radius.

For Model B, where the polymer concentration is uniformly distributed, and Model C, where the polymer flooding front radius is the same as the blockage radius, the interpretation of polymer flooding well tests can be divided into three steps. The matching curves are presented in Fig. 10, and the interpretation results are shown in Table 2.

Step 1: Input the basic parameters and pressure falloff test data of the test well into the calculation module based on the viscoelastic polymer flooding well test model developed in this paper.

Step 2: To reduce the time spent on curve matching, certain unknown parameters can be set within a range based on geological and production dynamic information from field examples.

Step 3: Adjust the unknown parameters based on the pressure response characteristics obtained from sensitivity analysis. For example, the curve characteristics of the wellbore section, transitional flow segment, and radial flow segment are very distinct and can help expedite the parameter adjustment process during history matching.

For Models A and D, which require consideration of the polymer flooding front radius, the well test interpretation steps are as follows:

Step 1: Assume a uniform polymer concentration of 0.503 kg/m^3 throughout the formation and perform well test matching using the viscoelastic polymer flooding well test model. Initially, the inner zone permeability of the formation is estimated to be 0.63 μm^2, the outer zone permeability is 2.13 μm^2, and the composite radius is 27 m.

Step 2: Based on the average injection rate and concentration during polymer injection, simulate two injection processes using the inner and outer zone permeabilities obtained in Step 1. The injection time is 362.7 d. Based on this, the polymer flooding front radius is estimated to be between 38 and 42 m (see Fig. 11).

Step 3: Fine-tune the polymer flooding front radius based on the estimation from Step 2 and adjust the magnitudes of the inner and outer zone permeabilities. The resulting polymer flooding front radius is 41 m, with an inner zone permeability of 0.42 μm^2 and an outer zone permeability of 1.09 μm^2.

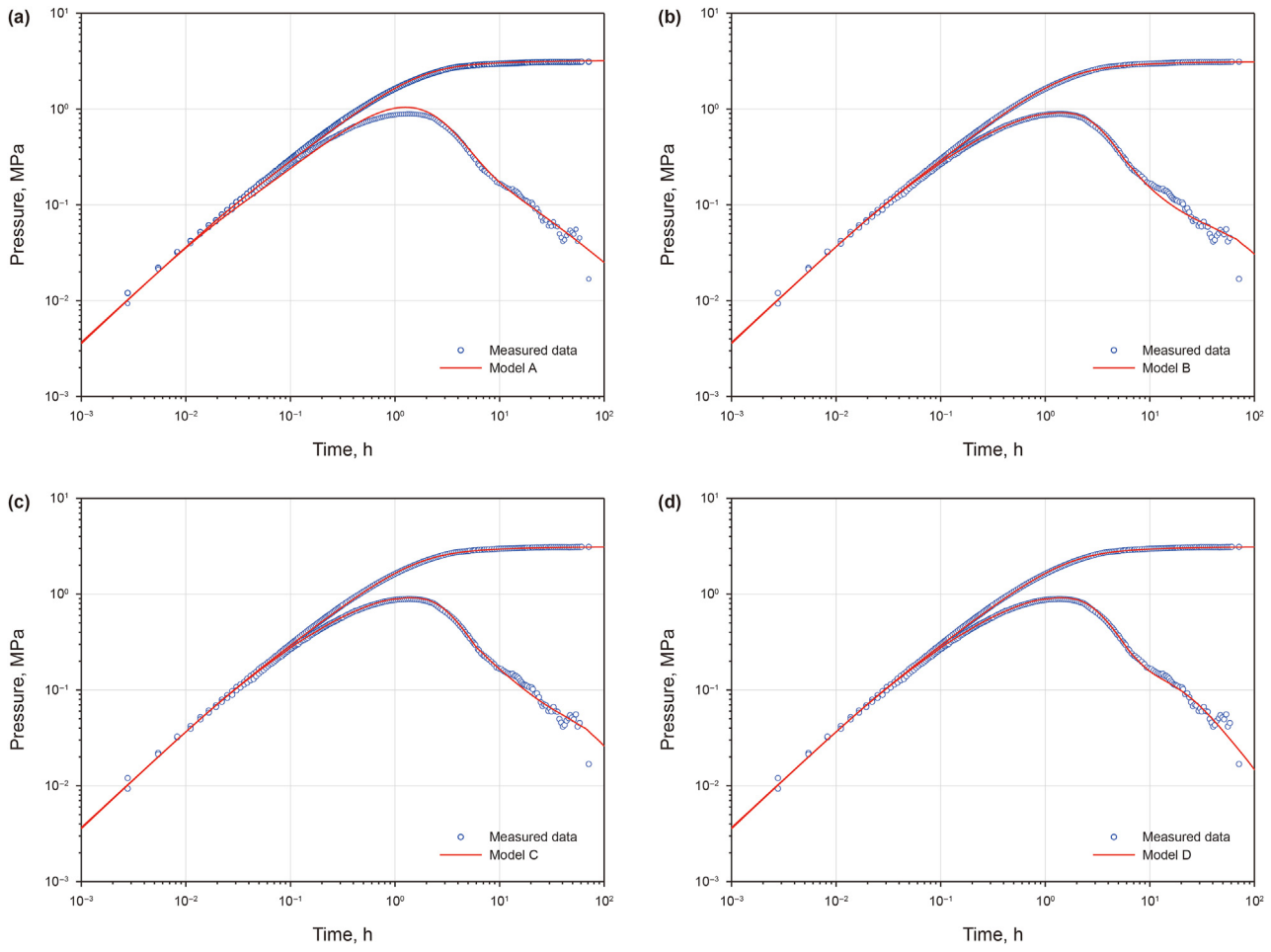

Fig. 10. History matching curves of four models.

Table 2
Interpretation results of four models for polymer flooding.

Model	Wellbore storage coefficient, m^3/MPa	Skin factor	Inner permeability, μm²	Outer permeability, μm²	Blockage radius, m	Polymer flooding front radius, m
Model A	0.92	2.06	0.42	1.09	27	41
Model B	0.92	−0.41	0.63	2.13	27	/
Model C	0.92	−0.41	0.63	1.26	31	31
Model D	0.92	−0.41	0.42	1.09	27	41

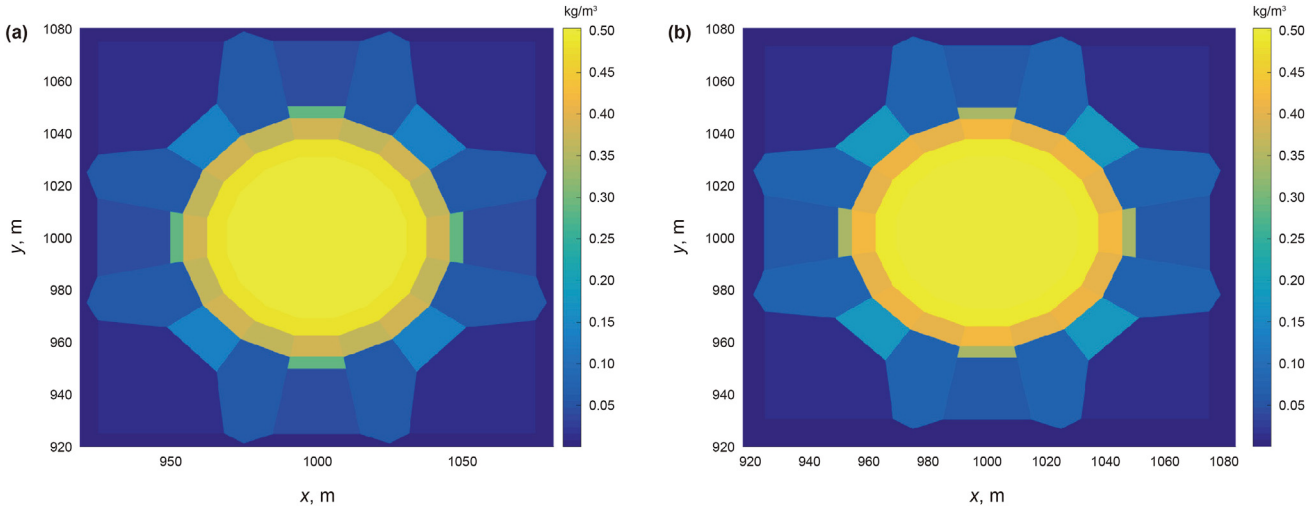

Fig. 11. Diagram of concentration gradient distribution of polymer flooding with different permeabilities: (**a**) 0.63 μm², (**b**) 2.13 μm².

For Model A, which does not consider the shear-thickening characteristics of the polymer, the matching effect of the transitional flow segment is not ideal, resulting in an overestimation of the skin coefficient in the interpretation. For Model B, which assumes a uniform distribution of polymer concentration, the matching results after the transitional flow segment are poor, leading to an overestimation of the outer zone permeability, significantly exceeding the average permeability of the area (0.786 μm²) and the well test interpretation results of adjacent test wells. As for Model C, where the polymer flooding front radius is the same as the blockage radius, both the inner and outer zone permeabilities interpreted are higher than those in Model D. However, for Model D, which considers polymer viscoelasticity and has different polymer flooding fronts and blockage radii, the matching effect is good (see Fig. 10 and Table 2). The interpreted well test results are consistent with the logging data and production dynamics. Compared with conventional well test for single-phase flow, this model is more accurate because it characterizes the complicated polymer behavior and considers the oil—water two phase flow. As a cost, the calculation speed of this model is slower. Therefore, it is recommended to explore methods or algorithms for optimization in the further research to enhance the model's computational efficiency.

5. Conclusions

(1) A two-phase numerical well testing model in viscoelastic polymer flooding is established considering the comprehensive effects of shear thickening, shear thinning, convection, diffusion, adsorption, retention, inaccessible pore volume, and reduced reservoir permeability caused by polymer solution in the porous media.
(2) The near-well blockage often occurs in polymer flooding wells, resulting in abnormally high injection pressure and injection difficulties. Different influence factors, including the degree of blockage (inner zone permeability), the extent of blockage (composite radius), and polymer flooding front radius are explored to investigate these impacts on bottom hole pressure responses.
(3) A field case is discussed to explore the necessity of considering polymer viscoelasticity in well test interpretation and the superiority of our viscoelastic polymer flooding numerical well test model in identifying near-well blockage in injection wells.

CRediT authorship contribution statement

Yang Wang: Methodology. **Shi-Long Yang:** Investigation. **Hang Xie:** Data curation. **Yu Jiang:** Software. **Shi-Qing Cheng:** Supervision. **Jia Zhang:** Writing — original draft.

Declaration of competing interest

The authors declare that they have no known competing financial interests or personal relationships that could have appeared to influence the work reported in this paper.

Acknowledgments

This work is supported by the National Natural Science Foundation of China (52104049), and the Young Elite Scientist Sponsorship Program by Beijing Association for Science and Technology (BYESS2023262).

References

Azad, M.S., Trivedi, J.J., 2019. Quantification of the viscoelastic effects during polymer flooding: a critical review. SPE J. 24 (6), 2731–2757. https://doi.org/10.2118/

195687-PA.
Bondor, P.L., Hirasaki, G.J., Tham, M.J., 1972. Mathematical simulation of polymer flooding in complex reservoirs. Soc. Petrol. Eng. J. 12 (5), 369–382. https://doi.org/10.2118/3524-PA.
Dauben, D.L., Menzie, D.E., 1967. Flow of polymer solutions through porous media. J. Petrol. Technol. 19 (8), 1065–1073. https://doi.org/10.2118/1688-PA.
Delshad, M., Magbagbeola, O.A., Huh, C., et al., 2008. Mechanistic interpretation and utilization of viscoelastic behavior of polymer solutions for improved polymer-flood efficiency. In: SPE Improved Oil Recovery Symposium. https://doi.org/10.2118/113620-MS.
Gringarten, A.C., 2008. From straight lines to deconvolution: the evolution of the state of the art in well test analysis. SPE Reservoir Eval. Eng. 11 (1), 41–62. https://doi.org/10.2118/102079-PA.
Hirasaki, G.J., Pope, G.A., 1974. Analysis of factors influencing mobility and adsorption in the flow of polymer solution through porous media. Soc. Petrol. Eng. J. 14 (4), 337–346. https://doi.org/10.2118/4026-PA.
Hou, J., Li, Z., Wang, Y., et al., 2003. Numerical simulation of polymer flooding with dispersion and adsorption. Chin. J. Comput. Phys. 20 (3), 239–244 (in Chinese).
Jennings, R.R., Rogers, J.H., West, T.J., 1971. Factors influencing mobility control by polymer solutions. J. Petrol. Technol. 23 (3), 391–401. https://doi.org/10.2118/2867-PA.
Kamal, M.M., Tian, C., Suleen, F., 2019. Pressure transient analysis of polymer flooding with coexistence of non-Newtonian and Newtonian fluids. SPE Reservoir Eval. Eng. 22 (3), 1172–1184. https://doi.org/10.2118/181473-PA.
Lake, L.W., Johns, R.T., Rossen, W.R., et al., 2014. Fundamentals of Enhanced Oil Recovery. Society of Petroleum Engineers. https://doi.org/10.2118/9781613993286.
Li, W., Liu, P., Li, Z., 2016. Establishment and application of well testing model considering variable skin factor. Fault-Block Oil Gas Field 23 (4), 492–496 (in Chinese).
Liang, G., Shen, P., Liao, X., 2016. Seepage flow and well test model for viscous-elastic polymer flooding reservoir. Journal of Southwest Petroleum University (Sci. Technol. Ed.) 38 (2), 136–142 (in Chinese).
Ma, Y., McClure, M.W., 2017. The effect of polymer rheology and induced fracturing on injectivity and pressure-transient behavior. SPE Reservoir Eval. Eng. 20 (2), 394–402. https://doi.org/10.2118/184389-PA.
Marshall, R.J., Metzner, A.B., 1967. Flow of viscoelastic fluids through porous media. Ind. Eng. Chem. Fundam. 6 (3), 393–400.
Masuda, Y., Tang, K.C., Miyazawa, M., et al., 1992. 1D simulation of polymer flooding including the viscoelastic effect of polymer solution. SPE Reserv. Eng. 7 (2), 247–252. https://doi.org/10.2118/19499-PA.
Meter, D.M., Bird, R.B., 1964. Tube flow of non-Newtonian polymer solutions: PART I. Laminar flow and rheological models. AIChE J. 10 (6), 878–881. https://doi.org/10.1002/aic.690100619.
Pye, D.J., 1964. Improved secondary recovery by control of water mobility. J. Petrol. Technol. 16 (8), 911–916. https://doi.org/10.2118/845-PA.
Qu, Z., Li, Y., Wang, L., 2019. Quantitative characterization methods of plugging position of offshore polymer flooding reservoir. Fault-Block Oil Gas Field 26 (3), 360–363 (in Chinese).
Seright, R.S., Wang, D., 2023. Polymer flooding: current status and future directions. Pet. Sci. 20 (2), 910–921. https://doi.org/10.1016/j.petsci.2023.02.002.
Shende, T., Niasar, V.J., Babaei, M., 2021. An empirical equation for shear viscosity of shear thickening fluids. J. Mol. Liq. 325, 115220. https://doi.org/10.1016/j.molliq.2020.115220.
Smith, F.W., 1970. The behavior of partially hydrolyzed polyacrylamide solutions in porous media. J. Petrol. Technol. 22 (2), 148–156. https://doi.org/10.2118/2422-PA.
Wang, Y., Cheng, S., Zhang, K., et al., 2019. Investigation on the transient pressure response of water injector coupling the dynamic flow behaviors in the wellbore, waterflood-induced fracture and reservoir: semi-analytical modeling and a field case. Int. J. Heat Mass Tran. 130, 668–679. https://doi.org/10.1016/j.ijheatmasstransfer.2018.09.083.
Wang, Y., Zhang, J., Yang, S., et al., 2024. Pressure transient characteristics of non-uniform conductivity fractured wells in viscoelasticity polymer flooding based on oil-water two-phase Flow. Pet. Sci. 21 (1), 343–351. https://doi.org/10.1016/j.petsci.2023.10.017.
Xie, Q., Xu, J., Chen, M., 2020. Unsteady pressure dynamics of polymer flooding reservoirs considering concentration changes. Chem. Technol. Fuels Oils 56 (3), 481–491. https://doi.org/10.1007/s10553-020-01159-x.
Yang, W., 2011. Transient Pressure Analysis of Viscoelastic Polymer Solution. Master Thesis. Northeast Petroleum University (in Chinese).
Yang, W., Yin, H., Zhong, H., et al., 2010. Well test analysis of viscoelastic polymer solution. J. Hydrodyn. 22 (1), 366–369. https://doi.org/10.1016/S1001-6058(09)60222-5.
Zhang, J., Cheng, S., Zhan, J., et al., 2021. The effect of rheology of viscoelastic polymer on pressure transient response in near-wellbore regions. Geofluids, 5568336. https://doi.org/10.1155/2021/5568336.